Energy & Environmental Science

Cite this: DOI: 10.1039/c2ee21548a

www.rsc.org/ees

PAPER

Effect of additional charging and current density on the performance of Capacitive energy extraction based on Donnan Potential†

Fei Liu,[ab] Olivier Schaetzle,[a] Bruno Bastos Sales,[ab] Michel Saakes,[ab] Cees J. N. Buisman[ab] and Hubertus V. M. Hamelers*[a]

Received 5th March 2012, Accepted 11th June 2012
DOI: 10.1039/c2ee21548a

The difference in the salt concentrations of river and seawater implies that wherever they mix, energy could be extracted from the salinity gradient. This is a renewable and clean means of generating energy that makes use of a natural process. Capacitive energy extraction based on the Donnan potential (CDP) is a promising technique for extracting this energy. We herein describe our investigation of the effect of additional charging on extraction behaviour using a forced current density. The study was conducted in a flow-through cell, using capacitive electrodes and ion exchange membranes. It is shown that increasing the accumulated charge in the system could be beneficial in terms of energy extraction. Furthermore, the addition of charge improved the power densities achieved. By charging at higher current densities and discharging at lower current densities, the performance of the system may be improved. The highest average power density achieved in this study was 0.205 ± 0.006 W m^{-2} (1.26 ± 0.75 mW g^{-1}). This was obtained using a charge of 6 C (4.62 C g^{-1}), with a controlled constant current of 50 mA (38.5 mA g^{-1} or 6.24 A m^{-2}). Three main limiting factors to the performance of CDP were identified, namely (i) the voltage drop over time, caused by the self-discharge of the cell and the non-ideal behaviour of the membranes, (ii) the duration of the switching times and (iii) the loss over the internal resistance. Of these, the internal resistance was identified as being the most important parameter to be minimized in order to further improve the performances of CDP systems.

Introduction

Salinity gradients present an emerging, renewable source of sustainable energy. There are no carbon dioxide emissions and no other by-products likely to have an impact on the global climate are produced. The natural process of mixing river water with seawater is intrinsically clean. The increase in entropy that results from the mixing of fresh and saline waters has considerable potential to provide significant quantities of clean energy (the technology is sometimes referred to as salinity gradient energy). The global power potential of salinity gradients has been estimated to be around 1.4 to 2.6 TW.[1–3] To put this in context, in 2009 the world's power consumption was 11.12 TW,[4] and it is thought that salinity gradient energy could potentially meet around 20% of global demand.

Several technologies have been developed to extract salinity gradient energy. The most well-known technologies are

[a]*Wetsus, Centre of Excellence for Sustainable Water Technology, Agora 1, P.O. Box 1113, 8900CC Leeuwarden, The Netherlands. E-mail: bert.hamelers@wetsus.nl; Fax: +31(0)5 8284 3001; Tel: +31(0)5 8284 3000*
[b]*Sub-Department of Environmental Technology, Wageningen University, Bornse Weilanden 9, 6708 WG Wageningen, The Netherlands*
† Electronic supplementary information (ESI) available: See DOI: 10.1039/c2ee21548a

Broader context

The world is in need of new energy sources that should be as renewable as possible and that are neutral regarding climate change. The mixing of seawater and river water leads to the dissipation of energy known as salinity gradient energy. The global potential of this renewable energy source is considerable (from 1.4 to 2.6 TW) and is not accompanied by the emission of any pollution and no greenhouse gasses are produced. Several technologies were proposed to exploit this energy source but so far none have effectively entered the energy market. Technical challenges should be addressed to have an efficient system that would be economically relevant. In this article, the authors present an improved and innovative method to extract this energy and directly convert it into electricity. Capacitive electrodes are used here in combination with ion exchange membranes to extract net energy from the mixing of a dilute saline solution with a concentrated saline solution.

pressure-retarded osmosis (PRO)[5,6] and reverse electro-dialysis (RED),[7–9] and substantial progress has been made in the development of these technologies in recent years. However, some problems remain in these energy harvesting techniques such as energy intensive pretreatments and pumping, fouling shortening the life of the operation and the need for energy converters. Recently, research has been carried out into new approaches to the extraction of salinity gradient energy, for example, the use of cation selective nanopores,[10] vapour pressure differences,[11] mechano-chemical processes,[12] electrochemical reactions,[13] and capacitive electrodes.[14–18]

The capacitive method is used to extract energy by charging capacitive electrodes in a concentrated saline solution, and discharging them in a dilute saline solution. The energy required to charge the electrodes is less than the energy extracted during the discharge, and it is therefore possible to extract part of the energy associated with the mixing of the system. There are two main methods for extracting salinity gradient energy, the first *via* Capacitive energy extraction based on Double-Layer Expansion (CDLE),[14–16] and the second through Capacitive energy extraction based on Donnan Potential (CDP).[14,17,18]

CDLE is a membrane-free process that arises from the expansion and contraction of the electrochemical double layer established on a capacitive electrode when the salt concentration changes. A constant potential is set during the charging and discharging steps that can be adapted in order to optimise the extraction of energy. By contrast, CDP involves the use of ion selective membranes that allow the development of the membrane equilibrium potential, also known as the Donnan potential.[19] In CDP, the Donnan potential is the driving force behind ion migration. The principal advantage of these technologies compared with PRO and RED is that the electricity generation is directly linked to the mixing process, so no additional intermediate energy conversions are necessary.

There are 4 steps in the charging and discharging process used to extract salinity gradient energy in both CDLE and CDP:

Step 1: Charging in a concentrated saline solution. The circuit is closed, which allows current to flow. The potential increases as charge is stored.

Step 2: Switching step. The concentrated saline solutions are replaced by a dilute saline solution with an open circuit. The cell potential increases, either due to double layer expansion in CDLE[14,15] or due to the establishment of the Donnan potential in CDP.[17,18]

Step 3: Discharging step in a dilute saline solution. The circuit is closed allowing the current to reverse.

Step 4: Switching step with an open circuit. This closes the cycle, and the dilute saline solution is replaced by the concentrated saline solution.

The charging step in CDP (step 1) can be realised without an external energy supply, with the Donnan potential being the driving force behind the migration of ions. This is known as an 'auto-generated cycle'. Alternatively, an external power supply can be used to force the charging cycle, supplying additional charge; this is referred to as a 'forced cycle'.

The relationship between the potential established and the charge accumulated, for both autogenerated and forced charging cycles, are shown in the energy cycle in Fig. 1. This cycle functions as a 4 step Carnot cycle and as such the area delimited by the arrows is a direct measure of the energy extracted during the cycle. More information on the way this cycle functions with respect to the invested and the extracted energy can be found in the ESI.† Two types of capacitive cycles are shown, one based on an 'auto-generated' process where the amount of charge is limited by the driving force of the Donnan potential, and one based on a 'forced' charging process where the system is charged beyond the limits of the Donnan potential. The darker area is a direct measure of the net energy extracted. In practice, two CDP cells could be connected such that cell 1 is discharging while charging cell 2. In the next cycle cell 2 is discharging while charging cell 1. In this way only an initial energy input is needed to make the system run. Therefore, the energy input is limited to the start-up of the initial cycle.

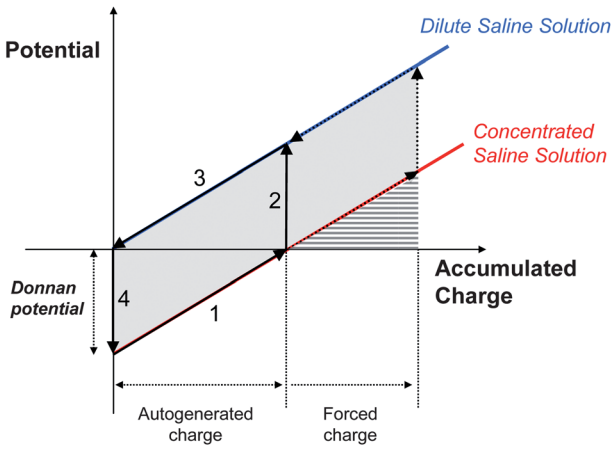

Fig. 1 Potential *vs.* charge relationship in ideal cycles (only with thermodynamic limitation) obtained by Capacitive energy extraction based on the Donnan Potential. Two types of capacitive cycles are shown, one based on an 'auto-generated' process where the amount of charge is limited by the driving force of the Donnan potential, and one based on a 'forced' charging process where the system is charged beyond the limits of the Donnan potential. The darker area is a direct measure of the net energy extracted per cycle and the stripped area is the energy invested in the forced charging cycle.

The first study of CDP focused on the auto-generated process[17] using a fixed external load. The aim of this study is to investigate if more energy and more power can be effectively extracted by forcing the charge of a CDP system and thus expanding the energy cycle as presented in Fig. 1. For this, a controlled current approach was selected in order to control the amount of charge exchanged in the process. Controlling the current rather than the potential as is done in CDLE studies,[14,15] allows a better management of the losses over the internal resistance and of the timing of the charging and discharging steps. The study of the effect of current density on the capacitive energy extraction was also achieved.

Moreover, a complete model describing the whole process was developed in this study. The model also reveals the limiting factors in a CDP system and leads to the direction for further research.

Materials and methods

Research setup

The CDP cell was operated as a lab-scale, flow-through cell, with 1 pair of electrodes and membranes assembled as shown in Fig. 2.

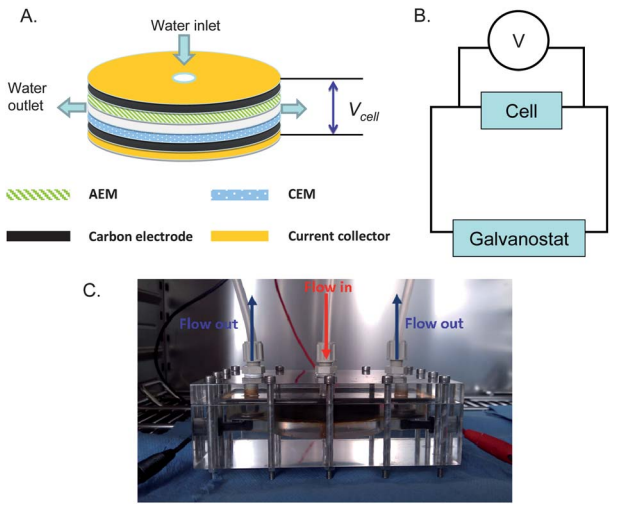

Fig. 2 Schematic drawing of one cell pair (A), the electric circuit that the cells are incorporated into (B), and a photograph of the cell, showing where the saline solutions enter and leave the cell (C).

The end plates of the stack consisted of two platinum coated (2.5 μm) titanium plate current collectors (Magneto special anodes B.V., NL, thickness = 375 μm). A layer of homemade, porous, activated carbon film (thickness = 270 μm) was placed on one side of each endplate, with the carbon film surfaces facing each other. The total mass of activated carbon material in the cell stack was 1.3 g, and the total geometric area of the electrode was 80.16 cm^2. An anion exchange membrane (AEM, Fumasep FAS, Fumatech, Germany, 30–40 μm), and a cation exchange membrane (CEM, Fumasep FKS, Fumatech, Germany, 30–40 μm), were placed in front of each activated carbon layer, as shown in Fig. 2A. A water flow channel was created between the membranes using a polymer spacer (PA 6.6 fabric, Nitex 03-300/51, Sefar, Heiden, Switzerland, thickness = 200 μm).

All the layers of the stack (see Fig. 2A) were disks 7.2 cm in diameter, which were pressed firmly into a PMMA (poly-methylmethacrylate) container. Saline solutions were pumped into the cell as required, through a circular hole of diameter 0.9 cm, located at the centre of the upper surface of the cell. The saline solutions spread symmetrically through the spacer layer, and flowed out of the cell in a perpendicular direction, through two outlets, as shown in Fig. 2A.

Capacitive electrodes

The porous carbon electrodes were made by mixing activated carbon powder with a binder solution. They were produced using the following method. Firstly, the carbon powder (DLC Super 30, Norit, Amersfoort, the Netherlands, BET area = 1600 $m^2 g^{-1}$) was dried in an oven at 105 °C for 24 h. Then, the carbon powder was mixed with a solution of polyvinylidene fluoride (PVDF; KYNAR HSV 900, Arkema Inc. Philadelphia, USA) in 1-methyl 2-pyrrolidone (NMP; Merck Schuchardt OHG, Hohenbrunn, Germany), in a ball mill grinder (PM 100, Retsch, Haan, Germany), for 30 min at 450 rpm. The resulting slurry was cast on a glass plate, using a 500 μm casting knife to produce a carbon film. The film was immersed in demineralised water in order to remove the remaining NMP. The final product was a solidified carbon film 270 μm thick, containing 10 wt% PVDF binder. The specific capacitance of the electrodes was 10.8 F g^{-1}.

Electrical measurement

In this study, the cell was connected in series with a galvanostat (IviumStat, Ivium Technologies, the Netherlands). The galvanostat was used to maintain a constant current (see Fig. 2B). The cell voltage was measured, and logged at 1 s intervals, using a Fluke digital multimeter (Fluke 8846A 6.5 digit precision multimeter, Fluke UK Ltd, Norwich, UK).

Operation and analysis

A synthetic concentrated saline solution (30 g L^{-1} NaCl) and a dilute saline solution (1 g L^{-1} NaCl) were alternately fed into the cell at a constant flow rate of 60 mL min^{-1}. All the experiments were carried out at 25 °C in a thermostatic incubator (Friocell, MMM Medcenter, Munich, Germany). Before the start of each experiment, the carbon electrodes were soaked in demineralised water to remove any remaining ions. The charging and discharging steps were conducted under a constant current.

In order to investigate the performance of our system under different charging regimes, we carried out charging and discharging using a constant current of 50 mA (38.5 mA g^{-1} of carbon electrode or 6.24 A m^{-2} of total geometric area). The amount of charge stored was controlled from 2 to 12 C (1.54 to 9.23 C g^{-1}) using steps of 2 C.

In this laboratory study, the conductivity change of the solution was not measured because the amount of ions exchanged during one cycle only account for less than 0.2% of the total ions present in the solution. However, this effect should be investigated in the case of a larger system as this could affect the internal resistance.

The four-step procedure described in the introduction was applied to this system. Before the first step of each cycle, the cell was short-circuited in order to achieve a potential of 0 mV in the dilute saline solution. The circuit was then opened and the solution was switched to the concentrated saline solution. When the cell reached a steady potential (of around −148 mV), the first (charging) step could begin. This charging procedure was used throughout this study and was necessary to be able to compare the different cycles. As such, consecutive cycles were not investigated in this study. Future investigations should focus on the different procedures for operating consecutive cycles.

Theory

We consider there to be four distinct components to the cell potential (eqn (1)):

(1) The membrane equilibrium potential (also known as the Donnan potential) E_m (eqn (2)), which is a function of the movement (activities) of the charged species into and out of the two membranes.

(2) The capacitive contribution to the potential E_e, (eqn (3)), which is a function of the capacitance of the system.

(3) The ohmic losses over the internal resistance IR_{int}.

(4) A potential drop over time $\Delta E_{leakage}$, which is related to the intrinsic self-discharge of the capacitive electrodes,[20] and to the non-ideal behaviour of the membranes.[21]

The foregoing components may be summarised in the equation:

$$E_{cell} = E_m + E_e - IR_{int} - \Delta E_{leakage} \quad (1)$$

where

$$E_m = -\frac{2\alpha RT}{nF}\ln\left(\frac{a_{sp}}{a_m}\right) \quad (2)$$

and

$$E_e = E_e^o + \frac{I}{C}t \quad (3)$$

E_{cell} is the cell potential measured between the two electrodes. E_m is the sum of the Donnan potentials from the sodium-ion and the chloride adsorption electrodes, and is a function of the activity of the ions in the spacer a_{sp} and the membrane a_m, the absolute temperature T, the average permselectivity of the membranes α, the gas constant R, the valence of salt ions n and the Faraday constant F (eqn (2)). E_e is the potential that relates to the amount of charge stored, and is defined in eqn (3), where E_e^o is the potential at the beginning of the charging or discharging step, I is the applied current, C the cell capacitance and t is the charging/discharging time. R_{int} is the internal cell resistance, and $\Delta E_{leakage}$ is a measure of the potential drop over time, which is related to the non-perfect selectivity of membranes[21] and to the self-discharge of the capacitor-like electrodes.[20]

Prior to step 1, the cell is completely discharged in the dilute saline solution *via* the shunting of the circuit ($E_m + E_e = 0$ mV). The water is then replaced with a concentrated saline solution at open circuit, which leads to a cell voltage of $E_{cell} \sim -148$ mV (assuming a permselectivity of 95%). The four-step CDP process does not begin until the steady state potential is reached.

Fig. 3A shows the potentials that our simple model (eqn (1)) describes, throughout a four-step charging and discharging operation. Fig. 3B shows experimental measurements of the cell potential with time, throughout the same four-step process. In Fig. 3, $\Delta E_{leakage}$ is assumed to be negligible because the amount of charge stored is relatively small, and the duration of the process is therefore relatively short.

During step 1 (closed circuit, concentrated solution), the cell is charged with a constant current I, which leads to an ohmic loss (IR_{int}), and a linear increase of the cell potential, which depends on the capacitance of the electrodes. At the end of this charging step, the circuit is opened (decreasing the ohmic loss contribution to zero). The concentrated saline solution is then replaced with a dilute saline solution.

During step 2 (open circuit, switching to dilute solution), the cell potential changes according to the new membrane potential E_m. As shown in Fig. 3A, the model does not describe the time t_{s1} required for achieving the membrane potential. The membrane potential is not achieved instantaneously, instead it takes several seconds to occur ($t_{s1} = 45.5 \pm 1.9$ s), when changing from a concentrated to a dilute solution. The measurements of switching time were done by measuring the time difference between the start of the potential rise and the time the potential reaches equilibrium. The complete replacement of the volume of water in the cell (the empty volume residence time) in our system only takes 0.8 s (0.8 mL replaced at a flow rate of 60 mL min^{-1}). This is

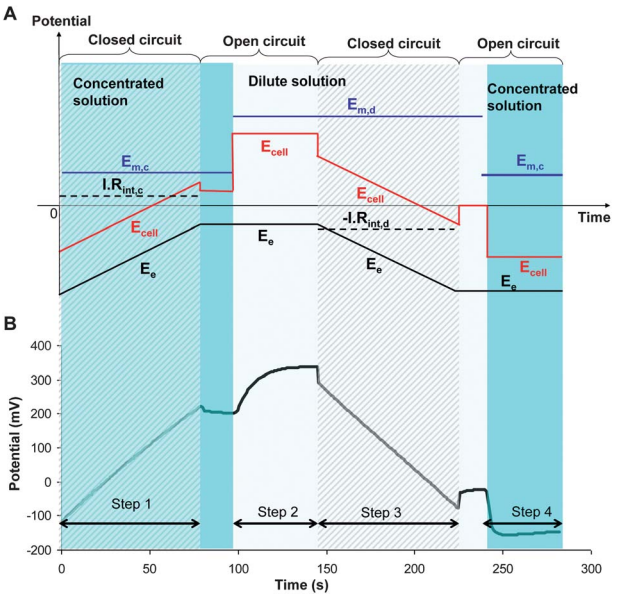

Fig. 3 (A) The cell potential throughout the charging and discharging process, described by the model given in eqn (1). The subscript c denotes the concentrated saline solution and the subscript d denotes the dilute saline solution. (B) Experimental data obtained from the system described in the Methods section. The 'lagging' periods between steps 1 and 2, and between steps 3 and 4, are not part of the operational cycle, but are shown to illustrate the contribution of the internal ohmic resistance.

insignificant compared to the time taken to establish the steady state membrane potential.

Step 3 (closed circuit, dilute solution) is similar to step 1 but with the reverse current and the same duration, in order to release the same amount of charge accumulated in the system during step 1. The model used to predict the potential follows the same linear progression that relates to the discharge of the capacitive electrodes. This may also be seen in the experimental data. The ohmic losses are more significant in step 3 than in step 1, because the dilute saline solution is less conductive.

Step 4 (open circuit, switching to concentrated solution) is the final switching step of the cycle, in which a concentrated saline solution replaces the dilute saline solution. Again, the membrane potential E_m, does not change instantaneously. In step 4, the membrane potential was established after $t_{s2} = 14.2 \pm 1.9$ s. This is considerably shorter than the time taken in step 2.

The present model provides a fair description of the four-step process, apart from in relation to the dynamics of the switching steps (steps 2 and 4). We observe two very interesting points. Firstly, the switching time is longer than the hydraulic residence time, indicating that mixing may not be the only factor that affects the time taken to achieve the Donnan potential. Secondly, we observe an asymmetric behaviour between steps 2 and 4. The switching time from a concentrated to a dilute solution was shorter than that from a dilute to a concentrated solution. These switching times represent more than 25% of the total time taken by the four steps, and their shortening is therefore an important step in increasing the power output of the system.

Our model also allows us to calculate the energy and power output during a single cycle by means of the following equation:

$$W_{net} = \int_{Q}^{0} E_{cell}^{D} dQ - \int_{0}^{Q} E_{cell}^{C} dQ \quad (4)$$

where

$$E_{cell}^{D} = E_{m,d} + E_{e}^{D} - IR_{int,d} - \Delta E_{leakage}^{D} \quad (5)$$

$$E_{cell}^{C} = E_{m,c} + E_{e}^{C} + IR_{int,c} - \Delta E_{leakage}^{C} \quad (6)$$

$$\Delta E_{leakage} = f(t) \quad (7)$$

The superscripts C and D represent the charging and discharging process. $R_{int,d}$ and $R_{int,c}$ are the internal cell resistances for dilute and concentrated saline solutions, respectively.

The net energy W_{net} can also be summarised in the equation:

$$W_{net} = W_{ext} - W_{IR} - \Delta W_{leakage} \quad (8)$$

Where W_{ext} is energy extracted in one cycle and W_{IR} is the energy loss over the internal resistance, and $\Delta W_{leakage}$ is the energy loss due to the potential drop over time.

The power is defined as:

$$P = \frac{W_{net}}{2t + t_{s1} + t_{s2}} = \frac{(\Delta E_m - IR_{int,sum})I}{2 + \frac{I(t_{s1} + t_{s2})}{Q}} - \frac{\Delta W_{leakage}}{2t + t_{s1} + t_{s2}} \quad (9)$$

where

$$R_{int,sum} = R_{int,d} + R_{int,c} \quad (10)$$

where t is the charging/discharging time, t_{s1} the switching time during step 2, t_{s2} the switching time during step 4, and $\Delta W_{leakage}$ is the energy loss due to the self-discharge and the non-ideal selectivity of the membrane. The $R_{int,sum}$ is the sum of the calculated internal resistances in concentrated saline solution and dilute saline solution.

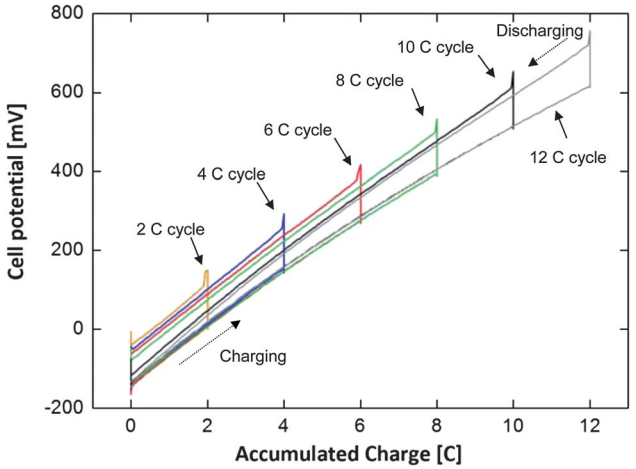

Fig. 4 The energy cycles obtained using different amounts of stored charge (2, 4, 6, 8, 10 and 12 C) for a constant current of 50 mA. The energy cycle started with the charging process at a cell voltage of $E_{cell} \sim -148$ mV. The standard deviation of repeated cycles is less than 5%, with the exception of 4 C cycles, in which the SD value is 6.1%.

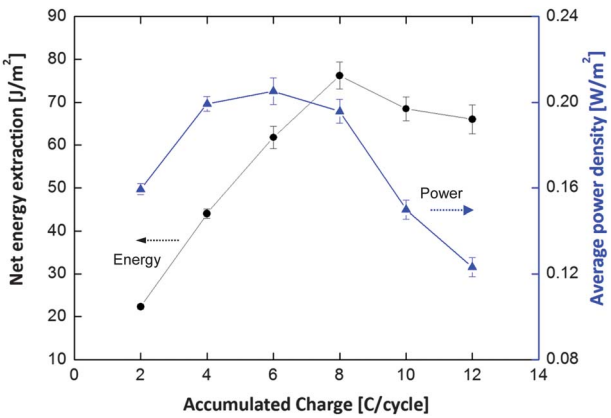

Fig. 5 Total energy extracted and average power density as a function of charge applied to the cell for a constant current of 50 mA.

Results and discussion

Effect of additional charging

Data obtained from a range of four-step operations in which the amount of stored charge was varied are shown in Fig. 4. These graphs show that the provision of additional charge in a CDP system leads to the extraction of a greater amount of energy. The greater the charge in the system, the more the area delimited by the coloured line expands horizontally. A greater amount of energy can therefore be extracted in a single operational cycle when a greater charge is stored.

As the amount of charge stored in the system increases, $\Delta E_{leakage}$ increases and is no longer negligible. $\Delta E_{leakage}$ occurs due to the non-ideal behaviour of the membrane and the self-discharge of the capacitor. The relationship between the cell potential and the accumulated charge is no longer linear.

The reproducibility of the system was tested by running the cycles in triplicate. An example of a 4 C cycle triplicate is available in the ESI.† The energy extracted and the average power density achieved per cycle, for accumulated charges of 2, 4, 6, 8, 10, and 12 C are plotted in Fig. 5. The energy extracted, presented here, is the difference between the energy harvested during the discharge and the (electrical) energy invested during the charge and does not take into account the energy losses due to the pumping and pretreatment of the solutions. These losses should be considered in future studies investigating the effect of mass transport and optimized flow rates. In comparable systems like reverse-electrodialysis, the pumping energy accounts for 25% of the total generated energy.[8] In theory, this number could be lower than 5%.[22] In comparison to a stack with spacers, the hydraulic losses were 4 times lower with the use of profiled membranes,[23] which can also be applied in CDP systems. The pretreatment in relation to stack design and operation has also been discussed in the RED system and the discussion pointed out a design towards a spacerless system.[22] As described in eqn (8), all the other losses including the leakages presented in Fig. 6 are taken into account.

The total energy extracted per cycle increased with the applied charge up to a maximum of 0.61 ± 0.02 J per cycle (0.47 ± 0.02 J g^{-1}

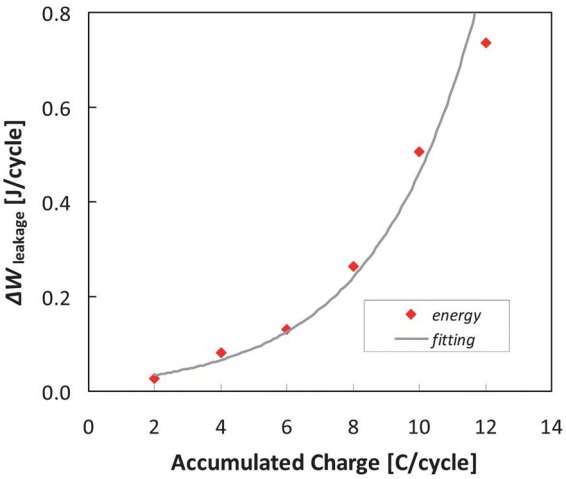

Fig. 6 Energy loss obtained from an exponential fit using experimental data.

per cycle or 76.1 ± 2.5 J m^{-2} per cycle) at 8 C (6.15 C g^{-1}). The average power density increased with accumulated charge up to a stored charge of 6 C (4.62 C g^{-1}) in the system. The power density was calculated per square meter of total geometric surface area of both electrodes. The maximum average power density was 0.205 ± 0.006 W m^{-2} (1.26 ± 0.75 mW g^{-1}). This is several orders of magnitude higher than the power density reported by Sales *et al.*[17] (0.007 W m^{-2} with 8 pairs of electrodes).

We have demonstrated that the forced charge process (when the system is charged beyond the limitations of the Donnan potential) leads to an improved performance of the system in terms of the amount of energy extracted and average power density, compared with the auto-generated process (at 2 C in this case). However, this increase in performance is limited by the fact that the drop in potential attributed to $\Delta E_{\text{leakage}}$ increases with accumulated charge. When the system is charged using a constant current, the time taken to achieve a particular charge increases with the value of the desired charge. $\Delta E_{\text{leakage}}$ is proportional to the charging time.

The voltage drop ($\Delta E_{\text{leakage}}$), and thus the resulting energy leakage, is difficult to define, because it is due to a number of phenomena, including the non-ideal behaviour of the membranes and the self-discharge of the capacitor-like electrodes. For this reason, we propose an empirical evaluation of the leakage in our system.

First, we evaluated the energy leaked during a 2 C cycle, and found it to be half the energy leaked during a 4 C cycle. We assume here that the amount of leaked energy is linear between 0 and 4 C; therefore we define the energy leakage at 2 C cycle ($\Delta W^{2C}_{\text{leakage}}$) using the following equation:

$$\Delta W^{2C}_{\text{leakage}} = 2W^{2C}_{\text{measure}} - W^{4C}_{\text{measure}} \quad (11)$$

The leakages for 4–12 C were defined using the following equation:

$$\Delta W^{x2C}_{\text{leakage}} = (W^{2C}_{\text{measure}} + \Delta W^{2C}_{\text{leakage}})x - W^{x2C}_{\text{measure}}, \quad x = 1, 2, \ldots, 6 \quad (12)$$

Fig. 6 shows the leaked energy for cycles in which different amounts of charge were applied. A relationship was obtained using an exponential fit ($R^2 = 0.9797$):

$$\Delta W_{\text{leakage}} = 0.018e^{0.3244Q} \quad (13)$$

We used our model to calculate the power density achieved under realistic conditions (incorporating energy leakage and actual switching times). The gray dashed line in Fig. 7 illustrates these results. Our model provides a good fit to the experimental data, and enables us to make theoretical predictions of cell performance.

If the leakage is prevented altogether, the power output will increase with the amount of charge applied as shown in Fig. 7 (gray solid line). This illustrates the benefit of using the forced charge process compared with the auto-generated cycle.

If the switching times are instantaneous ($t_{s1} = t_{s2} = 0$ s; but leakage still occurs), the power output will decrease in proportion to the amount of charge stored (black dashed line in Fig. 7). In this case there is a direct relationship between the amount of time taken to charge the system and the power density achieved. The greater the target accumulated charge, the longer the charging time. In this scenario, a longer charging time is simply less efficient than a shorter one. In this specific case, the addition of extra charge is no longer beneficial.

Finally, we consider instantaneous switching without leakage. In this case, there is a constant power output, whatever the amount of charge stored in the system (black solid line in Fig. 7). Here, the same amount of energy can be extracted from fewer cycles. This leads to an energy saving due to a reduction in the energy required to pump the solutions through the system.

The importance of the leakage effect was clearly shown in Fig. 7 by comparing the model with (gray dashed line) and

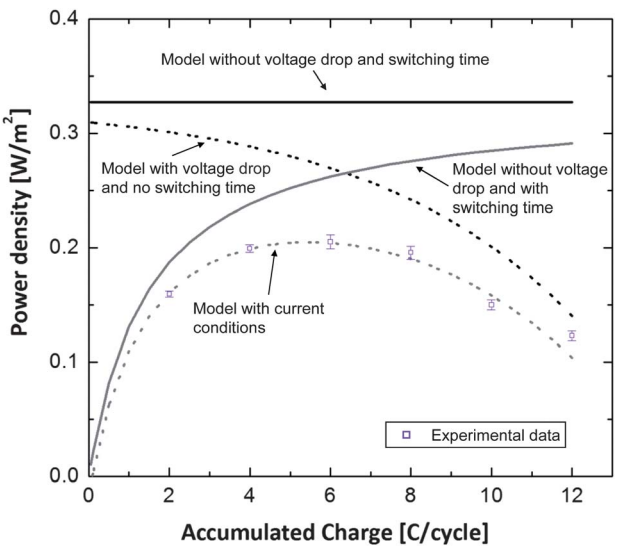

Fig. 7 Comparison of power density achieved in different theoretical scenarios. Experimental data are also shown (squares). The theoretical scenarios are: no leakage and $t_s = 60$ s (gray solid line), leakage and $t_s = 0$ s (black dashed line), leakage and $t_s = 60$ s (gray dashed line) and no leakage and with a zero total switching time $t_s = t_{s1} + t_{s2} = 0$ s (black solid line).

without (gray solid line) leakage. The theoretical scenario with predicted leakage (gray dash line) gives a good fit ($R^2 = 0.973$) with our experimental measurements, indicating a good estimation of the model on the leakage effect.

Further consideration is necessary to understand how the Donnan potential becomes established during the switching time, in order to minimise the duration of the process and thereby increase the power output. The mixing of the solutions alone cannot explain the long duration of the switching, because the hydraulic residence time is very short compared to the switching times ($t_{s1} = 45.5 \pm 1.9$ s, $t_{s2} = 14.2 \pm 1.9$ s). The asymmetry of the duration of switching times also supports this conclusion.

Fig. 7 indicates that the reduction of the voltage drop ($\Delta E_{leakage}$) and switching time leads to an increased power output. It also shows that the internal resistance is the limiting factor. Indeed, any improvements made to the leakage or the duration of the switching process will only allow the system to produce a maximum of 0.32 W m^{-2}. In order to increase the maximum output above this level, according to our model, the internal resistance and charge current should also be optimised. Improving the capacitance of the electrodes would allow higher charges to be accumulated in the system, but as Fig. 7 illustrates, the power density remains constant if the voltage drop ($\Delta E_{leakage}$) and switching times are zero. This leads us to conclude that it may be important to limit the voltage drop over the internal resistance in order to optimise this technology.

In the following section, we propose an optimisation procedure for our system using different current densities.

Effect of current density

We carried out a series of experiments in which our system was operated using different current densities. The cell was charged with controlled currents of ±20 mA (15.4 mA g^{-1} or 2.50 A m^{-2}), ±50 mA (38.5 mA g^{-1} or 6.24 A m^{-2}), and ±100 mA (76.9 mA g^{-1} or 12.48 A m^{-2}). The charging time was set so that 4 C (3.08 C g^{-1}) of charge was stored in the system. Fig. 8 presents the cell potential achieved as a function of the charge stored.

The energy extracted during each cycle was 0.463 J at 20 mA, 0.360 J at 50 mA, and 0.174 J at 100 mA. However, the duration of the process must be considered in order to compare the power output of these operating modes. Operation at 50 mA leads to an average power density of 0.186 W m^{-2} (1.15 mW g^{-1}) of the electrode (geometric surface), while operation at 20 mA leads to 0.123 W m^{-2} (0.76 mW g^{-1}) and that at 100 mA leads to 0.145 W m^{-2} (0.89 mW g^{-1}).

A closer inspection of the results shown in Fig. 8 shows that the charging step is more or less the same for the different current densities used. The conductivity of seawater is high enough to cause only a small variation in losses (IR_{int}) over the internal resistance (0.1 Ω) in this current range. In river water, however, the internal resistance is higher (0.7 Ω), which leads to higher losses at higher current densities. Therefore, the duration of the process can be optimised by charging at higher current densities and discharging at lower current densities. By charging at 100 mA and discharging at 50 mA, we were able to increase the power output by 30%.

Despite this operational optimisation, the losses over the internal resistance remain the major issue to resolve if the power

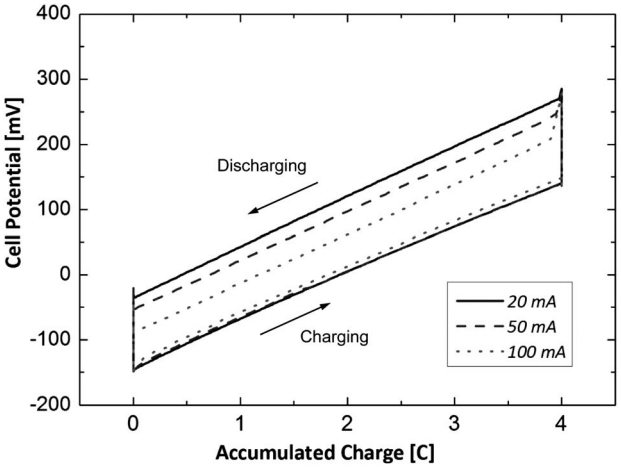

Fig. 8 Energy cycles with a 4 C charge loading, with controlled currents of 20 mA (15.4 mA g^{-1} or 2.50 A m^{-2}), 50 mA (38.5 mA g^{-1} or 6.24 A m^{-2}) and 100 mA (76.9 mA g^{-1} or 12.48 A m^{-2}).

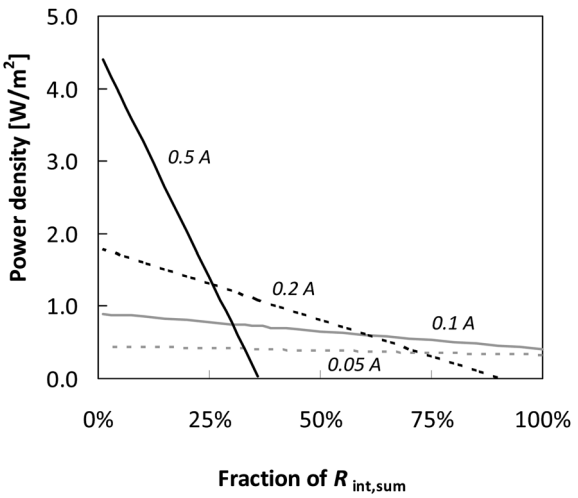

Fig. 9 Prediction of attainable power densities, in an ideal (no leakage and $t_s = 0$ s) CDP system using current densities of 0.05 A = 6.24 A m^{-2}, 0.1 A = 12.48 A m^{-2}, 0.2 A = 24.96 A m^{-2}, 0.5 A = 62.38 A m^{-2} and different internal resistances. The $R_{int,sum}$ is the sum of the calculated internal resistances in concentrated saline solution and dilute saline solution (0.7 Ω in dilute saline solution and 0.1 Ω in concentrated saline solution).

density of our system is to be improved. The power densities that could be reached by minimising the internal resistance are given in Fig. 9. In this figure, we have used our model to predict the power densities of an ideal system (no leakage and $t_s = 0$ s), with the internal resistance reduced to 75%, 50% or 25% of the internal resistance of our current experimental system, for different current densities. The $R_{int,sum}$ is the sum of the calculated internal resistances in concentrated saline solution and dilute saline solution (0.7 Ω in dilute saline solution and 0.1 Ω in concentrated saline solution).

Alternative technologies exist for extracting salinity gradient energy that are capable of achieving higher power densities than CDP systems. For example, a power density of 2 W m^{-2} was previously achieved using reverse electro-dialysis.[24] To reach

comparable power densities, CDP systems must lower their internal resistance by a factor of at least 4. This could be achieved by limiting all the contact resistances of the system, and by improving the conductivity of the capacitive electrodes.

Conclusions

In this paper, we have presented a study of how the capacitive energy of a CDP cell may be controlled by varying the accumulated charge and current density.

By controlling the amount of charge stored, we achieved an average power density of 0.205 ± 0.006 W m^{-2} (1.26 ± 0.75 mW g^{-1}) using a single pair of electrodes. This is several orders of magnitude higher than the power density reported by Sales *et al.*[17] (0.007 W m^{-2} with 8 pairs of electrodes). The forced charging process proved to be an effective means of increasing the capacitive energy.

We developed a model that provides a complete description of the cell potential throughout a charging and discharging cycle (see Fig. 3). Results generated using this model clearly illustrate the limitations of the system:

- Potential drop over time due to the intrinsic self-discharge of the capacitor-like electrodes and due to the non-ideal behaviour of the membrane.
- The switching time plays an important role in the cell performance.
- Ohmic losses due to the internal resistance of the system.

Among these, ohmic losses seem to be the most important to address in order to further improve the power output.

Further research is needed to optimize all of these parameters by limiting the leakages, optimizing switching times and by minimizing the ohmic losses.

List of symbols

a_m	Activity of the ions in the membrane
a_{sp}	Activity of the ions in the spacer channel
C	Cell capacitance, F g^{-1}
E_{cell}	Cell potential, mV
E_e	Capacitive electrode potential, mV
E_e^o	Potential of the capacitive electrode at the beginning of charging/discharging, mV
E_m	Membrane Donnan potential, mV
ΔE_m	Membrane Donnan potential difference, mV
$\Delta E_{leakage}$	Cell potential drop over time, mV
F	Faraday constant, C mole^{-1}
I	Applied current density, A m^{-2}
n	Valence of salt ions
P	Power density, W m^{-2}
Q	Accumulated charge, C per cycle
R	Ideal gas constant, J mol^{-1} K^{-1}
R_{int}	Internal cell resistance, Ω
$R_{int,sum}$	Sum of the calculated internal resistances in concentrated saline solution and dilute saline solution, Ω
t	Charging/discharging time, s
t_{s1}	Establishment of Donnan potential from concentrated saline solution to dilute saline solution, s
t_{s2}	Establishment of Donnan potential from dilute saline solution to concentrated saline solution, s
t_s	Total switching time, s
T	Absolute temperature, K
W_{ext}	Extracted energy, J per cycle
W_{IR}	Energy loss over internal resistance, J per cycle
$W_{measured}$	Extracted energy measured in the experiment, J per cycle
W_{net}	Net energy extraction, J per cycle
$\Delta W_{leakage}$	Energy loss, J per cycle

Subscripts

c	Concentrated saline solution
d	Dilute saline solution

Superscripts

C	Charging step
D	Discharging step

Acknowledgements

This work was performed in the TTIW-cooperation framework of Wetsus, Centre of Excellence for Sustainable Water Technology. Wetsus is funded by the Dutch Ministry of Economic Affairs, the European Union Regional Development Fund, the Province of Friesland, the City of Leeuwarden, and the EZ/Kompas program of the "Samenwerkingsverband Noord-Nederland". The present research has received funding from the European Union Seventh Framework Programme (FP7/2007-2013) under grant agreement no. 256868. The authors would like to thank the participants of the research theme "Blue Energy" at Wetsus for the fruitful discussions.

Notes and references

1 J. N. Weinstein and F. B. Leitz, *Science*, 1976, **191**, 557–559.
2 G. L. Wick and W. R. Schmitt, *Mar. Technol. Soc. J.*, 1977, **11**, 16–21.
3 G. Z. Ramon, B. J. Feinberg and E. M. V. Hoek, *Energy Environ. Sci.*, 2011, **4**, 4423–4434.
4 IEA, *Key World Energy Statistics*, International Energy Agency, Paris, 2011.
5 T. Thorsen and T. Holt, *J. Membr. Sci.*, 2009, **335**, 103–110.
6 A. Achilli, T. Y. Cath and A. E. Childress, *J. Membr. Sci.*, 2009, **343**, 42–52.
7 J. W. Post, H. V. M. Hamelers and C. J. N. Buisman, *Environ. Sci. Technol.*, 2008, **42**, 5785–5790.
8 J. Veerman, M. Saakes, S. J. Metz and G. J. Harmsen, *J. Membr. Sci.*, 2009, **327**, 136–144.
9 P. Długołęcki, A. Gambier, K. Nijmeijer and M. Wessling, *Environ. Sci. Technol.*, 2009, **43**, 6888–6894.

10 W. Guo, L. Cao, J. Xia, F.-Q. Nie, W. Ma, J. Xue, Y. Song, D. Zhu, Y. Wang and L. Jiang, *Adv. Funct. Mater.*, 2010, **20**, 1339–1344.
11 M. Olsson, G. L. Wick and J. D. Isaacs, *Science*, 1979, **206**, 452–454.
12 M. V. Sussman and A. Katchalsky, *Science*, 1970, **167**, 45–47.
13 F. La Mantia, M. Pasta, H. D. Deshazer, B. E. Logan and Y. Cui, *Nano Lett.*, 2011, **11**, 1810–1813.
14 D. Brogioli, *Phys. Rev. Lett.*, 2009, **103**, 058501–058504.
15 D. Brogioli, R. Zhao and P. M. Biesheuvel, *Energy Environ. Sci.*, 2011, **4**, 772–777.
16 N. Boon and R. van Roij, *Mol. Phys.*, 2011, **109**, 1229–1241.
17 B. B. Sales, M. Saakes, J. W. Post, C. J. N. Buisman, P. M. Biesheuvel and H. V. M. Hamelers, *Environ. Sci. Technol.*, 2010, **44**, 5661–5665.
18 B. B. Sales, F. Liu, O. Schaetzle, C. J. Buisman and H. V. Hamelers, *Electrochim. Acta*, 2011, DOI: 10.1016/j.electacta.2012.05.069, in press.
19 F. G. Donnan, *J. Membr. Sci.*, 1995, **100**, 45–55.
20 Q. Zhang, J. Rong, D. Ma and B. Wei, *Energy Environ. Sci.*, 2011, **4**, 2152–2159.
21 X. J. Meng, Q. L. Liu, A. M. Zhu and Q. G. Zhang, *J. Membr. Sci.*, 2010, **360**, 276–283.
22 J. W. Post, C. H. Goeting, J. Valk, S. Goinga, J. Veerman, H. V. M. Hamelers and P. J. F. M. Hack, *Desalin. Water Treat.*, 2010, **16**, 182–193.
23 D. A. Vermaas, M. Saakes and K. Nijmeijer, *J. Membr. Sci.*, 2011, **385–386**, 234–242.
24 D. A. Vermaas, M. Saakes and K. Nijmeijer, *Environ. Sci. Technol.*, 2011, **45**, 7089–7095.